Volume 10
Number 10
14 March 2022
Pages 5003–5652

Journal of Materials Chemistry A

Materials for energy and sustainability

rsc.li/materials-a

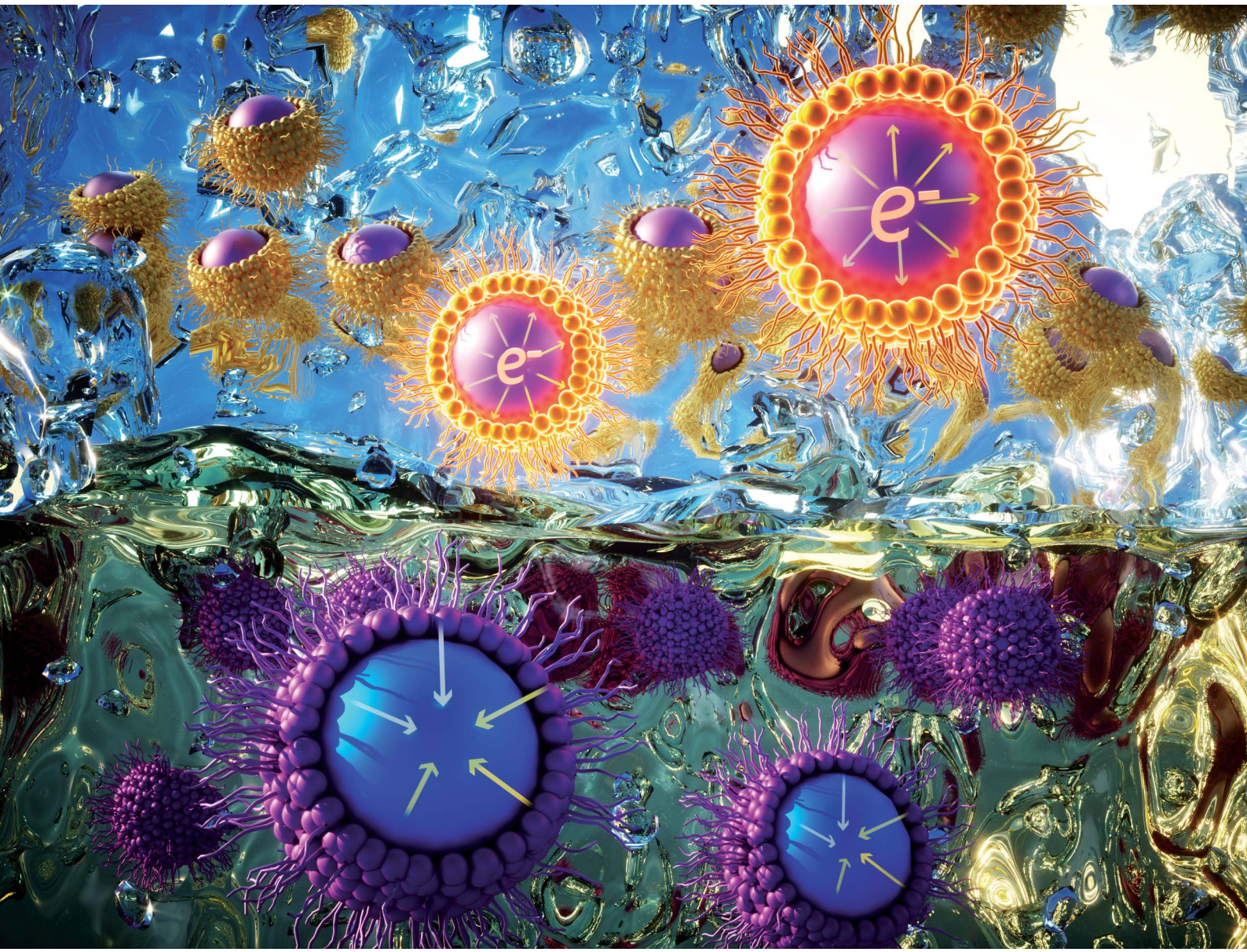

ISSN 2050-7488

ROYAL SOCIETY OF CHEMISTRY

PAPER

Sergei Tretiak, Dibyajyoti Ghosh *et al.*

Nature of electronic excitations in small non-stoichiometric quantum dots

Journal of Materials Chemistry A

ROYAL SOCIETY OF CHEMISTRY

PAPER

View Article Online
View Journal | View Issue

Cite this: *J. Mater. Chem. A*, 2022, **10**, 5212

Nature of electronic excitations in small non-stoichiometric quantum dots†

Manav Bhati, [abc] Sergei A. Ivanov, [de] Thomas P. Senftle, [c] Sergei Tretiak [*abe] and Dibyajyoti Ghosh [*abef]

Colloidal quantum dots (QDs) have emerged as nanocrystalline semiconductors with tunable optoelectronic properties that have attracted attention for numerous commercial applications. While a significant amount of computational research has focused on understanding the stoichiometric QDs, most of the experimental synthesis techniques lead to non-stoichiometry in QD composition. In this work, we utilize time-dependent density functional theory to investigate the nature of electronic excitations in experimentally relevant non-stoichiometric cadmium selenide (CdSe) nanoclusters in a dielectric medium. Contrary to the stoichiometric QDs, we find a distinct charge transfer character for low-energy electronic excitations in non-stoichiometric QDs. This partial charge transfer occurs between the core and surface of QDs due to the charge imbalance originating from the inequivalent number of anionic and cationic atoms in these regions. This general phenomenon, accompanied with charge localization, results in optically dark low-energy transitions that would potentially hamper emissions in non-stoichiometric QDs, especially in anion-rich QDs. The insights from this study establish relationships between the optical properties and charge distributions in non-stoichiometric QDs that would facilitate their tunability for various applications.

Received 16th September 2021
Accepted 8th December 2021

DOI: 10.1039/d1ta07983b

rsc.li/materials-a

Introduction

Colloidal II–VI and III–V semiconductor quantum dots (QDs) have found their applications in a broad range of technologies[1–3] such as solar cells,[4–6] light-emitting diodes (LED),[7–9] biological imaging,[10–12] photocatalysis,[13–15] and quantum computing.[16,17] The ability to modify the functionalities of these QDs by precisely tuning their size and combining multiple semiconducting materials in a single nanocrystal underpin these applications.[18] In addition, the facile and economical synthesis[19] has encouraged the commercial adoption[20,21] of colloidal QD-based technologies. However, these materials are still in an early stage of commercialization due to their inconsistent and non-uniform size distribution during large-scale synthesis, being far from producing the idealized atomically identical structures. Conventional synthesis techniques[22] for colloidal QDs face challenges in dealing with uniformity and reproducibility of specific structural and chemical features, leading to inconsistencies in quantum yields and fluorescence efficiencies from batch to batch. As-synthesized, QDs generally are far from their archetype stoichiometric counterparts, both in terms of stoichiometry and photophysical properties,[23] that are highly sensitive to their surface composition and ligand capping, thus negatively impacting fluorescence efficiencies. The surface-associated transitions, which are the main culprits, remain unnoticed and difficult to characterize *via* experiments as they are optically forbidden.[24] Instead, atomistic simulations have proven to be a powerful tool to identify and explore the photophysics of such transitions. Several simulation techniques, ranging from the adiabatic ground state to non-adiabatic excited-state calculations, have been applied to understand the photo-chemo-physical properties of QDs in detail.[25–28] However, most of these attempts[29–37] have focused on stoichiometric QDs (with an equal number of cation and anion atoms) that are less frequently obtained from the conventional synthesis. The more common non-stoichiometric QDs, with cation-to-anion ratios deviating from one, that are critical to many optical and photocatalytic applications, remain largely unexplored. Significance of non-stoichiometry in QDs is highlighted well by Huang *et al.*[38] as they demonstrated a 10-fold increase in photocatalytic H_2 evolution upon decreasing surface

[a]*Theoretical Division, Los Alamos National Laboratory, Los Alamos, NM, 87545, USA. E-mail: serg@lanl.gov; dibyajyoti@iitd.ac.in*

[b]*Center for Nonlinear Studies, Los Alamos National Laboratory, Los Alamos, NM, 87545, USA*

[c]*Department of Chemical and Biomolecular Engineering, Rice University, 6100 Main Street, Houston, TX 77005-1892, USA*

[d]*Materials Physics and Applications Division, Los Alamos National Laboratory, Los Alamos, New Mexico, 87545, USA*

[e]*Center for Integrated Nanotechnologies, Los Alamos National Laboratory, Los Alamos, NM, 87545, USA*

[f]*Department of Materials Science and Engineering, Department of Chemistry, Indian Institute of Technology Delhi, Hauz Khas, New Delhi 110016, India*

† Electronic supplementary information (ESI) available. See DOI: 10.1039/d1ta07983b

Se composition from ~16.7% to ~4.9% in CdSe QDs. In another study on photocatalytic reduction of CO_2 to CO,[39] decreasing surface Se from 20.71% to 7.38% in CdSe QDs resulted in 92-fold enhancement in CO production. Yet, it is not well understood what modifications of electronic structure in such QDs assist in improving the catalytic performance.

Non-stoichiometry of a QD gives rise either to positively charged cation-rich or to negatively charged anion-rich nanocrystals (assuming the presence of neutral ligands on the surface). Among the limited computational studies of non-stoichiometric QDs, most have explored cation-rich QDs[40–44] and with very little focus on their anion-rich counterparts.[45,46] In addition, most of the computational investigations of non-stoichiometric QDs have been carried out in the gas phase,[43,44,46] whereas synthetic manipulations and experiments on QDs are mostly conducted in solutions or other dielectric media,[22] increasing the disparity between the outcomes of computational modeling and experimental results on their optical properties. It has been also well established that the incorporation of solvation effects into modeling can drastically alter the predicted optical properties of studied nanocrystalline systems. Given the presence of a dielectric medium around a QD, the energetics of the surface-associated orbitals get stabilized, leading to the removal of the in-gap states and thereby often increasing the oscillator strengths of the lowest transitions.[31,47–49] Chemically, the overall non-zero charge of a non-stoichiometric QD can usually be compensated by charge-neutralizing ligands on the QD surface. However, from the modeling perspective, the availability of multiple sites on the QD surface for ligand placement significantly increases the complexity and structure diversity as these sites are non-identical in terms of ligand binding.[47] In addition, ligand displacement has been observed experimentally,[50,51] which could expose different sites on the QD surface in an experimental system. Existing modeling studies that have investigated non-stoichiometric QDs, rarely consider the effect of different placement of the same number of ligands around the same QD, making the conclusions less general. Given all these concerns, it is important to investigate the non-stoichiometric QDs, especially anion-rich species, in a more relevant and uniform simulation framework.

In this computational study, we aim to address these issues to bridge the knowledge gap between stoichiometric and non-stoichiometric QDs. We attempt to elucidate the nature of surface-associated electronic excitations in small non-stoichiometric CdSe QDs (~15 Å in diameter) by examining both cation-rich (Cd-rich) and anion-rich (Se-rich) QDs. Time-dependent density functional theory (TDDFT) in conjunction with a Conductor-like Polarizable Continuum Model (CPCM)[52,53] is applied to simulate absorption spectra of non-stoichiometric QDs in a dielectric medium (acetone). We find that the inclusion of the solvent effects is crucial in stabilizing the polar surface orbitals and removing several low-energy dark states. We also investigate the effects stemming from various surface ligand arrangements around the same QD structure on the optical properties of QDs by modeling absorption spectra of several non-stoichiometric QDs with inequivalent ligand placement configurations. Overall, we determine that electronic excitations with a pronounced charge transfer character dominate the low-energy optical transitions in non-stoichiometric QDs, and anion-rich QDs exhibit poor emissive characteristics compared to that of cation-rich QDs.

Results and discussion

We consider three types of QD clusters: two non-stoichiometric (see insets in Fig. 1a) and one stoichiometric (see inset in Fig. S1a†). The non-stoichiometric structures are either Se-rich ($Cd_{17}Se_{28}H_{22}$) or Cd-rich ($Cd_{28}Se_{17}Cl_{22}$) and both are initially related to each other *via* switching of cation/anion placement. Initial geometries of these structures had T_d symmetry and the hybrid wurtzite/zinc blende arrangement of Cd and Se atoms: vertices of the tetrahedron had a wurtzite arrangement whereas the center of the cluster was in the zinc blende configuration with respect to the rest of the QD. For comparison, we also consider previously studied (both experimentally and theoretically) stoichiometric $Cd_{33}Se_{33}$ structure. Our computational results for this stoichiometric system are presented in ESI materials.† The Se-rich and the neutral clusters have been experimentally characterized in previous studies.[54–56] In the non-stoichiometric QDs, H^+ and Cl^- in the Se-rich and Cd-rich dots, respectively, serve as charge-neutralizing ligands to balance the overall charge on the ligated nanocluster. To speed up quantum-chemical simulations in the Se-rich system, C_6H_5-moiety (present in the experimental structure)[55,57] was replaced with H^+. Electronegative nature of C_6H_5-moiety assists in neutralizing excess electron density on anion-rich QDs. A charge-neutralizing H^+ ligand achieves a similar function in these QDs. As such, H^+ binds to the anionic Se atoms whereas in the Cd-rich QD, Cl^- binds to the cationic Cd atoms. Our electronic structure calculations start with geometry optimizations followed by excited state and absorption spectra simulations. All computational details are provided in the Methods section.

Fig. 1a shows calculated absorption spectra of the Se-rich and Cd-rich QDs in acetone (top row) as a red curve with individual transitions highlighted in the blue line-stick plot. In these spectra, we focus on two electronic excitation states denoted as S_1 and S_{max}. S_1 is the first singlet excited state, which is qualitatively responsible for the luminescence properties of the QD. In contrast, S_{max} is the excited state with the maximum oscillator strength across all calculated transitions and is representative of the absorption properties of the QD in the low-energy region. In the experimental absorption spectra, the lowest energy excited states with very low oscillator strength (*e.g.*, optically dark S_1) are often not detectable or difficult to assign.[25] Therefore, the S_{max} presented here should be compared with the first pronounced peak in the experimental absorption spectra. The S_{max} of Se-rich QD (3.43 eV) is in good agreement with the first peak of previously reported experimental absorption spectra (~3.5 eV) of same-size Se-rich QD.[54] The S_{max} of the Cd-rich QD (2.91 eV) is red-shifted because of the larger size of Cd-rich QD and greater coupling of Cl^- ligands with the QD wavefunction (see below). In addition, the S_{max} (2.93 eV) of stoichiometric $Cd_{33}Se_{33}$ QD (see ESI Fig. S1†) agrees

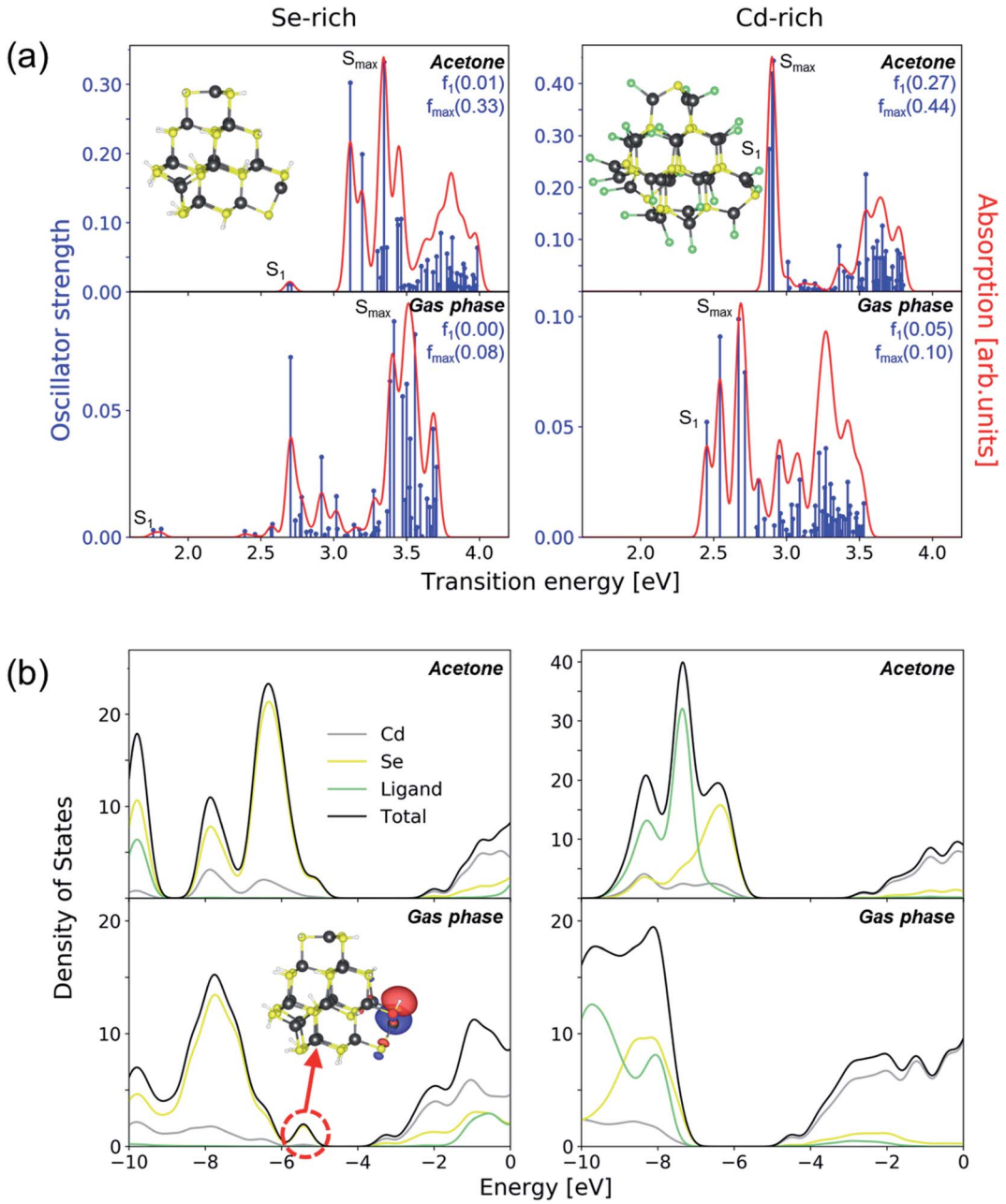

Fig. 1 (a) Calculated absorption spectra of the Se-rich and Cd-rich quantum dots in acetone (top row) and in the gas phase (bottom row). The absorption spectra (shown in red) are obtained from the Gaussian convolution of the line-stick spectra (shown in blue) with 0.035 eV line-broadening parameter (see Methods). The insets show the respective atomic structures of the quantum dots. Atoms in yellow: Se, grey: Cd, white: H, green: Cl. The first electronic transition state is marked as S_1 and the state with maximum oscillator strength is denoted as S_{max}. The oscillator strengths of these two states are written in blue in the top right corner of the plots as f_1 and f_{max}, respectively. (b) Partial density of states (PDOS) plots of the Se-rich and Cd-rich QDs in acetone (top row) and gas phase (bottom row) delineating contributions of Cd, Se, and ligand atomic orbitals. The inset in the PDOS of Se-rich QD in the gas phase shows the Kohn–Sham orbital of the in-gap trap state.

well with the experimental lowest energy absorption peak (~2.99 eV) of $Cd_{33}Se_{33}$ QD.[56]

The first peak, S_1, of the Se-rich QD is weaker (reflecting the presence of less optically active transitions) compared to that of the Cd-rich QD. This observation agrees with previous experimental studies, showing that Se-rich QDs have poorer luminescence compared to Cd-rich QDs.[46,58] The cause of the weak first transition in Se-rich QD is believed to be the presence of trap states in the bandgap.[43,46,59] However, as shown in Fig. 1b (top row), we do not observe any pronounced mid-gap states in both Se-rich and Cd-rich QDs in acetone. Similar results were published in a recent work for stoichiometric QDs in the gas phase,[36] where the dark (*i.e.*, optically forbidden) states were present in the electronic spectra but without the obvious appearance of trap states in the bandgap. Here, for the Se-rich QD in the gas phase, a definite in-gap state does appear near

the valence band edge. Upon plotting the charge density of the Kohn–Sham orbital of this trap state, we find that it is localized on the undercoordinated surface Se-atom, as shown in the inset of Fig. 1b. We note that not all surface atoms are passivated with ligands as the number of ligands is constrained by the charge neutrality of the ligated QD. Importantly, for both types of QDs, the states in the valence and conduction band are mostly comprised of Se and Cd atomic orbitals, respectively, as shown by the PDOS plots in Fig. 1b and the orbital plots discussed below. Therefore, the trap state in Se-rich QD in the gas phase appears on the Se atom. Similar trap states are not present in the Cd-rich QD as most of the Se atoms are inside the core and are fully coordinated, thereby resulting in a better emission.

The trap state in the bandgap of the Se-rich QD affects its optical properties by quenching the fluorescence due to trap-assisted non-radiative recombination. This is evident from the appearance of several low-energy excitations in the absorption spectra of this QD (Fig. 1a), particularly pronounced in the gas phase simulations. The same effect but to a lesser degree is observed in Cd-rich or stoichiometric (see ESI Fig. S1†) QDs because of the absence of trap states in the bandgap computed in the gas phase. These results underscore the importance of including solvent effects into QD simulation models as gas-phase results over exaggerate the appearance of spurious low-energy dark states due to the lack of a stabilizing dielectric medium around the QD.[36] Owing to the electrostatic nature of solvation effects, they are expected to be particularly significant in non-stoichiometric QDs as the electron density in the latter is more polarized due to the charge imbalance in QD core. The solvent screens the polarization, stabilizing the surface-associated orbitals. This consequently lowers their energies thereby widening the bandgap and removing mid-gap states. In the above example of the Se-rich QD, the in-gap trap state obtained in the gas phase appears as a shoulder in PDOS calculated in acetone, Fig. 1b (which may still negatively affect the emission as computed absorption spectrum shows). To adhere to a more physical model, our discussion below will involve only solvated QDs.

As an electron–hole pair is formed during optical excitation, the charge densities of the excited electron and hole can be obtained from the natural transition orbital (NTO) analyses[60] of the electronic excitations. The distribution of these electron and hole densities over atoms can be further quantified by the inverse participation ratio (IPR), which is calculated as follows

$$\mathrm{IPR} = \frac{1}{\left(N\sum_{i=1}^{N}\rho_i^{\,2}\right)}$$

where, ρ_i is the density of either electron or hole on atom i, and N is the total number of atoms in the system. Here, we use Hirshfeld charges[61] as the measure of electron and hole densities on each atom. The IPR quantifies the degree of charge delocalization over all the atoms. In the limiting case of maximum delocalization, where the charge density is equally shared by all the atoms, *i.e.*, $\rho_i = 1/N$, the IPR attains its maximum value equal to 1. The opposite limit of IPR is $1/N$ when the charge density is strictly localized on just one atom (say atom a), *i.e.*, $\rho_{i=a} = 1$ and $\rho_{i\neq a} = 0$. The natural transition

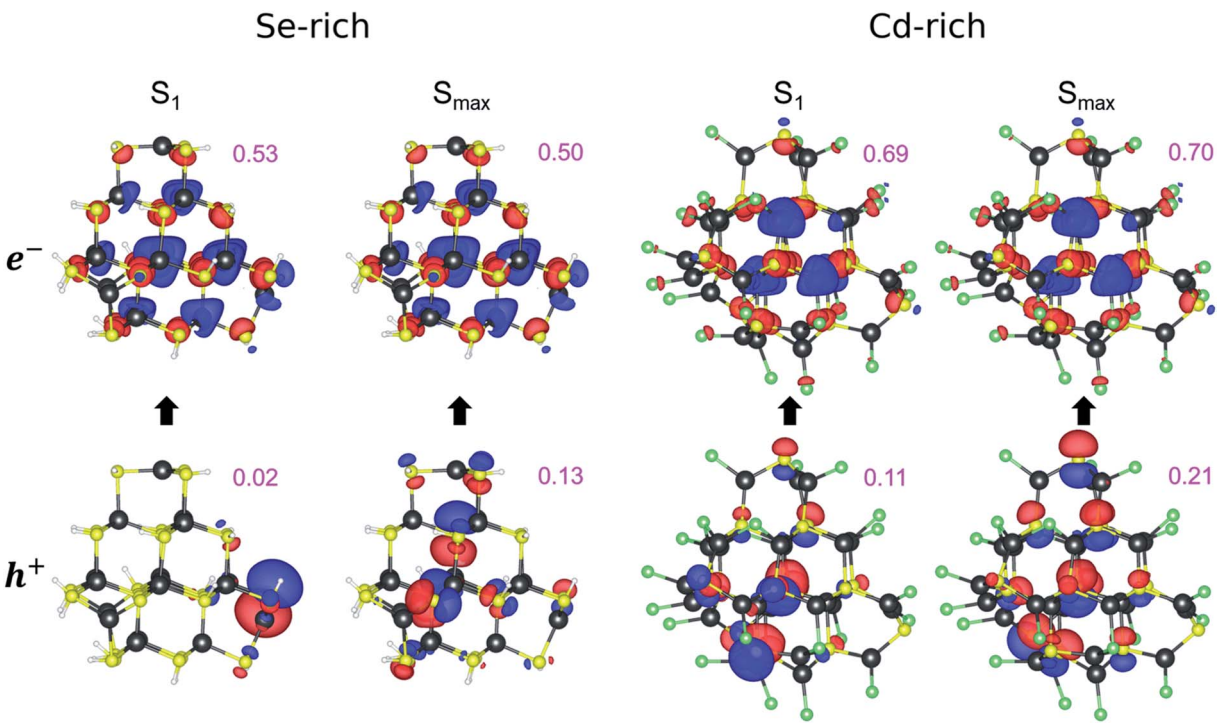

Fig. 2 The natural transition orbitals (NTO) of electron (top row) and hole densities (bottom row) of S_1 and S_{max} states of the Se-rich and Cd-rich QDs. The isosurface values of 0.016 e Å^{-3} and 0.020 e Å^{-3} were used to generate the isosurfaces for the electron and hole density plots, respectively. The inverse participation ratio (IPR) value for each NTO is shown in pink.

orbitals (NTOs) of electron and hole densities along with the respective IPR for S_1 and S_{max} of the Se-rich and Cd-rich QDs are shown in Fig. 2 and the same for the stoichiometric QD are shown in ESI Fig. S2.† In all the QD structures, most of the hole and electron densities appear on Se and Cd atoms, respectively. This is concomitant to PDOS plots in Fig. 1b reflecting the composition of valence and conduction orbitals. Furthermore, the electron density is more delocalized as compared to the hole density in all excited states considered, as shown by the IPRs. It is also evident that NTO distributions and IPR values are closely related. For highly localized charge densities, such as the hole density in S_1 of Se-rich QD, the IPR is small (and approaches 0.015 or 1/67, where $N = 67$ atoms in this QD). The specific oscillator strengths of the excited states can also be related to IPRs. In general, the IPRs for S_{max} are higher than those for S_1, suggesting a higher level of delocalization, which would lead to a better overlap of electron and hole wavefunctions in the S_{max} excited state and thus a higher oscillator strength. Compared to stoichiometric QDs (Fig. S2†), the localization of charges is higher in non-stoichiometric QDs (smaller IPR), suggesting that non-stoichiometric QDs would be more reactive and suitable for photocatalytic applications.

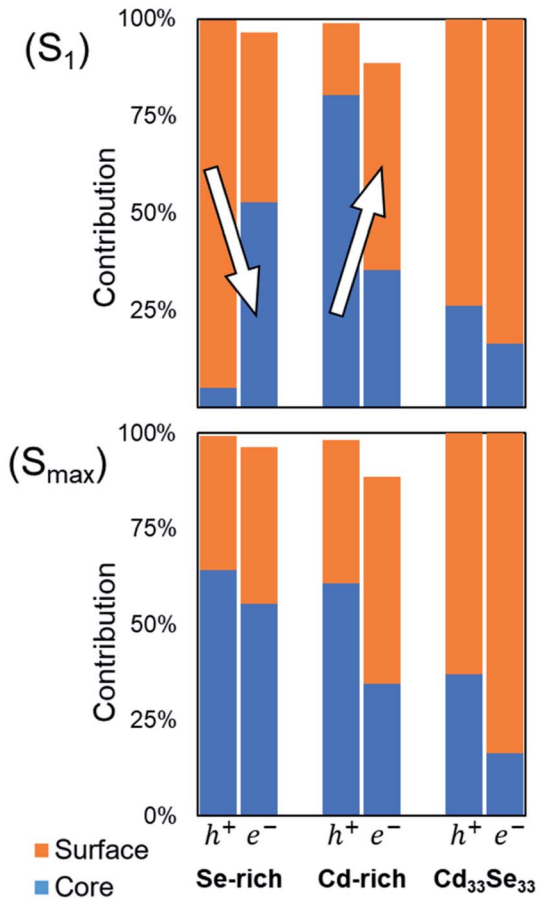

Fig. 3 The relative contributions of surface (orange) and core (blue) atoms into electron and hole transition orbitals for S_1 and S_{max} transitions in non-stoichiometric Se-rich, Cd-rich, and stoichiometric $Cd_{33}Se_{33}$ quantum dots. The arrows represent the direction of charge transfer: surface-to-core in Se-rich QD and core-to-surface in Cd-rich QD.

The nature of S_1 and S_{max} excitations can also be described in terms of electron and hole densities distributions over the core and surface atoms of the QD (Fig. 3). Here, we define the core atoms as an atom with a coordination number of four, and the rest Cd/Se atoms are considered as the surface atoms. The dominant contribution to excited electron and hole densities comes from Cd and Se atoms with only a small part ascribed to the ligand atoms (H in Se-rich, and Cl in Cd-rich QDs). We find that in non-stoichiometric QDs, the low-energy transition, S_1, has a significant charge transfer (CT) character: CT is directed from the surface to the core in the Se-rich QD and the opposite direction in the Cd-rich QD. We believe that the main cause of the CT character is the charge imbalance in the non-stoichiometric QD between the surface and core in the ground state. Subsequently, we summate all Hirshfeld[61] charges across the respective class of atoms and find that in the Se-rich QD, total charges on all surface and core atoms amount to $-0.8e$ and $+0.8e$, respectively, whereas, in the Cd-rich QD, the charges on surface and core are $+0.4e$ and $-0.4e$, respectively. Notably, to have an overall zero net charge on the entire QD in this analysis, the charge on ligand atoms is included in the charge on surface (Cd/Se) atoms. This qualitative measure of the charge imbalance defines the direction of CT, from a region with high electron density to a region with a low one due to optical excitation.

This CT character also complies with the observations from Fig. 1b and 2. Since most of the holes are created on Se atoms (due to a higher contribution of Se orbitals to the valence band), the placement of Se atoms determines the origin of holes on the photoexcited QD. Because of the non-stoichiometry, most Se atoms are present on the surface of the Se-rich QD, where the holes are originated. In contrast, the holes originate in the core for the Cd-rich QD. The opposite situation but to a lesser extent holds for electrons, which are generally much more delocalized. This provides an alternative rationale for the direction of CT. These insights also underpin reasoning for the poor emission properties of Se-rich QDs. As electrons tend to be more delocalized as compared to holes (Fig. 2), the placement of Se atoms (or holes) determines the degree of charge delocalization. Since most Se atoms are located on the surface of Se-rich QD, they tend to be more are exposed and sensitive to an immediate chemical environment compared to those in Cd-rich QDs, and therefore, have a weaker hole delocalization, resulting in a poor overlap of electron–hole wavefunctions and weak oscillator strength.

Unlike non-stoichiometric QDs, the charge imbalance in $Cd_{33}Se_{33}$ is significantly lower ($+0.1e$ and $-0.1e$ on surface and core, respectively). As such, the S_1 excitation occurs over the entire QD (Fig. S2†) and does not drive a flow of electrons from one region to another (Fig. 3), resulting in non-CT bulk-type transition. The transitions with high oscillator strength (S_{max}) are also non-CT in nature for all 3 nanoclusters considered, being examples of the bulk-type transitions. Here the electron and hole wavefunctions in the excited state have a significant overlap (thus maximizing oscillator strength), which is not

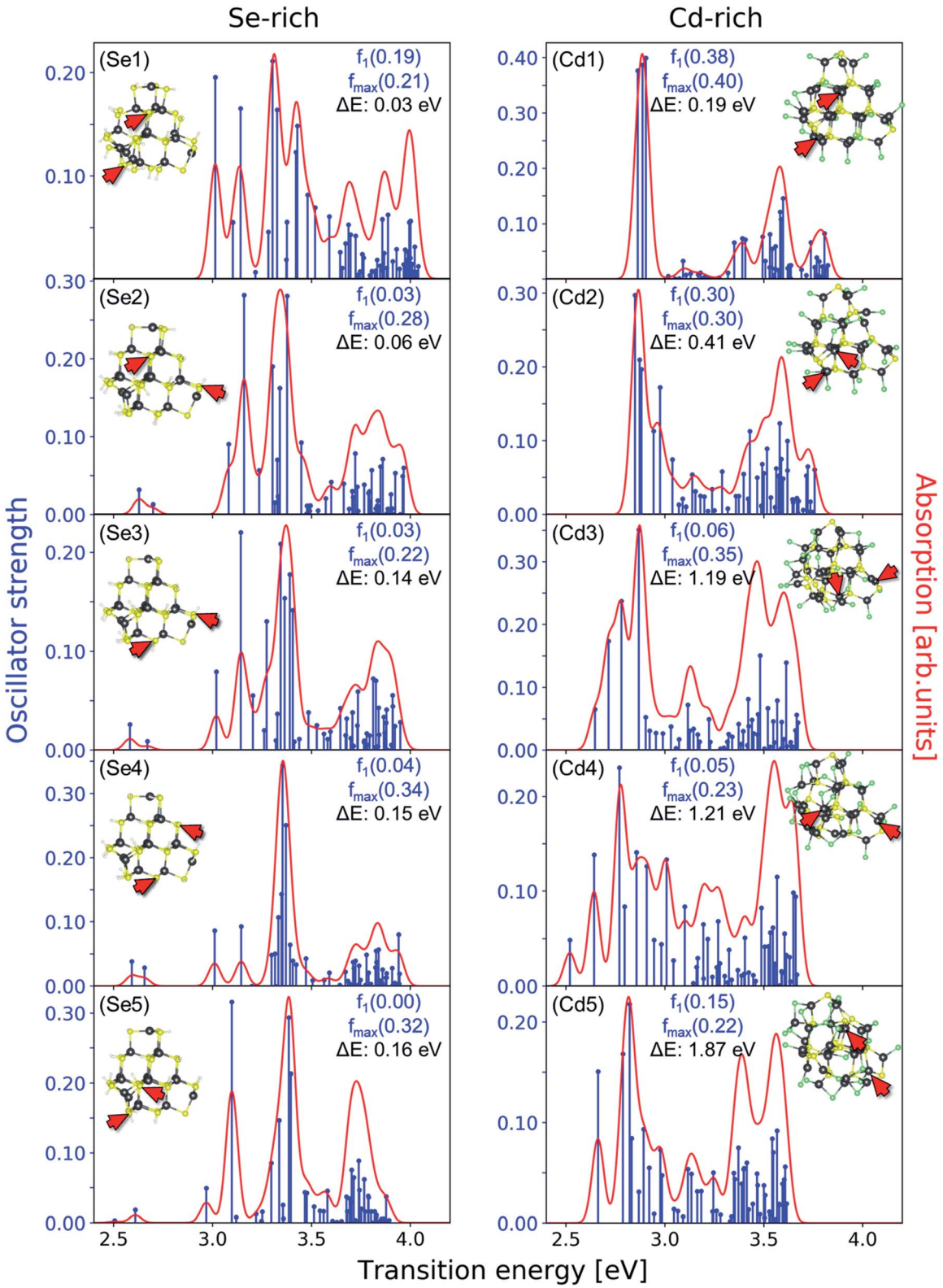

Fig. 4 The absorption spectra of various Se-rich (**Se1–5**) and Cd-rich (**Cd1–5**) QDs along with their atomic structures in the insets were calculated using the same approach as used in Fig. 1a. The position of atoms that were non-ligated (without ligand capping) before the geometry optimization is represented with the red arrows. Atoms in yellow: Se, grey: Cd, white: H, green: Cl. In the top right corner of each plot, the oscillator strengths (in blue font) of the excited state with the lowest energy (f_1) and that with maximum oscillator strength (f_{max}) are shown along with the ground state energy difference, ΔE (in black font) between the corresponding QD structure and the one of the same type shown in Fig. 1.

possible in a CT type transition. Therefore, the S_{max} transitions in all types of QDs are similar as shown in Fig. 3.

Having understood the nature of electronic excitations in non-stoichiometric QD structures presented in Fig. 1, it is important to verify if these results remain valid for other ligand configurations of these QDs. In the non-stoichiometric QDs that we have considered here, two atoms on the surface (two Se in the Se-rich QD and two Cd in the Cd-rich QD) are not bonded to any ligand. The number of ligands is determined from the net charge of the QD and is therefore restricted, leaving two surface atoms bare (without ligands) for the QDs considered here. Such difference between the number of surface coordination sites and the number of ligands brings about an issue of the non-unique arrangement of available ligands on the QD surface, giving rise to multiple ligand configurations on the surface. There are several chemically viable configurations for selecting two non-ligated bare surface atoms in these QDs, but they all fall under one of the three categories (see Fig. S3† for more details): (i) each bare atom is bonded to just core atoms, (ii) each bare atom is bonded to both core and surface atoms, (iii) one bare atom is bonded to just core atoms and another to surface and core atoms. For each of the three categories, we created two candidate QD structures with different placement of ligands, exposing different inequivalent bare surface atoms. Investigating these six non-equivalent ligand configurations for each Se-rich and Cd-rich QDs helps us draw general conclusions that are qualitatively valid for a family of non-stoichiometric QDs. Geometry optimizations and absorption spectra evaluations of the six structures for each type of non-stoichiometric QDs were performed using the solvation model framework. Five of these spectra are shown in Fig. 4 (**Se1–5** and **Cd1–5**), and one (with the lowest ground state energy) is already discussed in Fig. 1. Along with the spectra, optimized QD structures and their energy differences (ΔE) relative to the respective lowest energy ligand configuration (shown in Fig. 1) are listed. Observed variations of the absorption spectra suggest that the optical properties of non-stoichiometric QDs are sensitive to the surface configuration and ligand placement. This is similar to the sensitivity of QD electronic properties to different kinds of ligands or defects on the surface.[24] In general, the S_{max} peak, which represents the absorption characteristics remains essentially the same for each Se-rich and Cd-rich QD structure considered. However, the S_1 peak, changes significantly for different structures, suggesting a greater influence of surface structure on the emission properties if compared to the absorption properties of non-stoichiometric QDs. In particular, most of the Se-rich QD structures and their spectra are thermally accessible (due to small ΔE), demonstrating a higher likelihood of poor emissions in the Se-rich QDs. On the other hand, the low-energy structures of the Cd-rich QDs (**Cd1–2**), have similar spectra with high S_1 peaks, demonstrating a higher likelihood of better emission in the Cd-rich QDs. These results support previous experiments that highlight that anion-rich non-stoichiometric QDs are likely to have poor fluorescence quantum yields.[58]

We note that the size of the QDs considered in this study (~15 Å in diameter) is on the lower limit of the experimentally synthesized QDs.[62] The size would change the surface-to-volume ratio of QDs, which might affect the magnitude and quantity of CT-like transitions. Still, the fluorescence of larger anion-rich and cation-rich QDs synthesized experimentally[58] are different and these differences can be qualitatively explained by our results.

In experiments, an identical distribution of ligands over QD surface is difficult to achieve. Furthermore, the ligand mobility[41] is likely to give rise to the co-existence of several ligand configurations at the same time. Such inhomogeneity in surface ligand configurations is often overlooked in computational simulations, where a single ligand arrangement is utilized to draw generalized results. By investigating several ligand arrangements, we attempted to address this experimental scenario of surface ligand configuration variability; however, we did not undertake an exhaustive search for all possible surface ligand configurations in the three categories mentioned above. Despite that, our results allow for several qualitative claims about the nature of electronic excitations persisting across surface ligand configurations considered, as discussed above. Furthermore, for most of the Se-rich (Cd-rich) structures, the CT occurs from surface to the core (from core to surface) in the lowest energy S_1 transition, as shown in ESI Fig. S4.† The direction of charge transfer suggests that under photoexcitation, the Se-rich and Cd-rich QD would have a higher density of holes and electrons on the surface, respectively, making them potentially suitable as photooxidation and photoreduction catalysts, respectively. This rationalizes the enhanced photocatalytic activity of H_2 and CO_2 reductions upon increasing the Cd content in CdSe QDs in the previous experiments.[38,39] Our future efforts will focus on further exploration of the photocatalytic properties of non-stoichiometric QDs and developing strategies to improve their emission characteristics.

Conclusion

In this computational study, the nature of electronic excitations in small non-stoichiometric QDs (~15 Å in diameter) is characterized and found to be distinct from their stoichiometric counterparts. The imbalance of anionic and cationic atoms in non-stoichiometric QDs results in charge imbalances between the core and surface of QD, which promote charge localization and charge transfer phenomena. As such, the low energy transitions in non-stoichiometric QDs exhibit a pronounced CT character, where the electronic charge transfers from surface to core in the Se-rich QD and from core to surface in Cd-rich QD. Moreover, the presence of excess Se on the surface of Se-rich QDs favors surface-localized hole wavefunctions for low-energy excitations. This underpins decreased overlap of electron–hole wavefunctions, resulting in poor emission characteristics of Se-rich QDs. These results hold when multiple surface ligand configurations are considered: several inequivalent arrangements of ligands on the QD surface exhibit similar electron/hole localizations and CT character. The CT phenomena, in conjunction with a localized surface charge density, in non-stoichiometric QDs, especially Se-rich ones, would not be ideal for emissive applications but would be

promising for photocatalytic applications. Additionally, the possibility of multiple ligand configurations on QD surface should not be overlooked when modeling ligated non-stoichiometric QDs, as it might lead to incorrect over-generalization of identified electronic features onto all possible QD configurations. Obtained insights on the nature of charge carrier excitations in non-stoichiometric QDs provide guidelines toward strategic modifications of these nanocrystalline materials for various applications ranging from efficient quantum emitters to photocatalysts.

Computational methods

All the QD structures were optimized to their ground state minima using density functional theory (DFT) as implemented in the Gaussian16 (ref. 63) software package. The optimized structures have the forces and energies converged within the default Gaussian values. B3LYP[64,65] hybrid exchange–correlational functional was used along with LANL2DZ[66–68] basis set for Cd and Se, and 6-31-G* basis set for H and Cl atoms. The effective core potential (ECP) was applied for Cd and Se atoms, for which 12 and 6 electrons, respectively, were treated as valence electrons. To minimize computational expense, QD structures were first relaxed in the gas phase before optimizing in acetone (solvent phase), utilizing a Conductor-like Polarizable Continuum Model (CPCM).[52,53] For excited-state calculations, we employed time-dependent density functional theory (TDDFT) to obtain the excitations of the first 50 electronic transitions. The absorption spectra were derived from the line spectra by applying Gaussian convolution with a full width at half maximum of 0.035 eV. Such computational methodology has been extensively tested and used across a broad variety of previous modeling studies.[31,35,36,47,69,70] Hirshfeld[61] charge analysis, as applied in Multiwfn[71] v3.7 software package, was used to obtain the charge distribution on all the atoms and calculate the Inverse Participation Ratios (IPRs). We obtained the partial density of states (PDOS) plots from Gaussian outputs using GaussSum software package[72] and visualized atomic structures and orbitals using the VESTA[73] v3.5.7 software.

Data availability

Results from all the calculations on stoichiometric ($Cd_{33}Se_{33}$) QD and additional configurations of non-stoichiometric QD supporting this article have been described in the manuscript and are provided in an ESI.†

Conflicts of interest

There are no conflicts to declare.

Acknowledgements

The work at Los Alamos National Laboratory (LANL) was supported by the Laboratory Directed Research and Development (LDRD) program at LANL under project 20200213DR. This work was done in part at the Center for Nonlinear Studies (CNLS) and the Center for Integrated Nanotechnologies (CINT), a U.S. Department of Energy and Office of Basic Energy Sciences user facility, at LANL. This research used resources provided by the LANL Institutional Computing Program. Los Alamos National Laboratory is operated by Triad National Security, LLC, for the National Nuclear Security Administration of the U.S. Department of Energy (Contract No. 89233218NCA000001). All authors thank Dr Victor I. Klimov for fruitful discussions.

References

1 F. P. G. de Arquer, D. V. Talapin, V. I. Klimov, Y. Arakawa, M. Bayer and E. H. Sargent, *Science*, 2021, **373**, eaaz8541.
2 M. A. Cotta, *ACS Appl. Nano Mater.*, 2020, **3**, 4920–4924.
3 J. M. Pietryga, Y.-S. Park, J. Lim, A. F. Fidler, W. K. Bae, S. Brovelli and V. I. Klimov, *Chem. Rev.*, 2016, **116**, 10513–10622.
4 Z. Pan, H. Rao, I. Mora-Seró, J. Bisquert and X. Zhong, *Chem. Soc. Rev.*, 2018, **47**, 7659–7702.
5 G. H. Carey, A. L. Abdelhady, Z. Ning, S. M. Thon, O. M. Bakr and E. H. Sargent, *Chem. Rev.*, 2015, **115**, 12732–12763.
6 R. D. Schaller and V. I. Klimov, *Phys. Rev. Lett.*, 2004, **92**, 186601.
7 V. L. Colvin, M. C. Schlamp and A. P. Alivisatos, *Nature*, 1994, **370**, 354–357.
8 Y. Shirasaki, G. J. Supran, M. G. Bawendi and V. Bulović, *Nat. Photonics*, 2013, **7**, 13–23.
9 W. K. Bae, Y.-S. Park, J. Lim, D. Lee, L. A. Padilha, H. McDaniel, I. Robel, C. Lee, J. M. Pietryga and V. I. Klimov, *Nat. Commun.*, 2013, **4**, 2661.
10 Z. Yue, F. Lisdat, W. J. Parak, S. G. Hickey, L. Tu, N. Sabir, D. Dorfs and N. C. Bigall, *ACS Appl. Mater. Interfaces*, 2013, **5**, 2800–2814.
11 S. Mallick, P. Kumar and A. L. Koner, *ACS Appl. Nano Mater.*, 2019, **2**, 661–666.
12 M. J. Molaei, *RSC Adv.*, 2019, **9**, 6460–6481.
13 Y. Zhou, S. Yang, D. Fan, J. Reilly, H. Zhang, W. Yao and J. Huang, *ACS Appl. Nano Mater.*, 2019, **2**, 1027–1032.
14 R. L. Calabro, D.-S. Yang and D. Y. Kim, *ACS Appl. Nano Mater.*, 2019, **2**, 6948–6959.
15 F. E. Osterloh, *Chem. Soc. Rev.*, 2013, **42**, 2294–2320.
16 D. Loss and D. P. DiVincenzo, *Phys. Rev. A: At., Mol., Opt. Phys.*, 1998, **57**, 120–126.
17 C. R. Kagan, L. C. Bassett, C. B. Murray and S. M. Thompson, *Chem. Rev.*, 2021, **121**, 3186–3233.
18 L. Liu, Q. Peng and Y. Li, *Inorg. Chem.*, 2008, **47**, 5022–5028.
19 K. J. Nordell, E. M. Boatman and G. C. Lisensky, *J. Chem. Educ.*, 2005, **82**, 1697.
20 X. Dai, Y. Deng, X. Peng and Y. Jin, *Adv. Mater.*, 2017, **29**, 1607022.
21 D. Graham-Rowe, *Nat. Photonics*, 2009, **3**, 307–309.
22 Y. Pu, F. Cai, D. Wang, J.-X. Wang and J.-F. Chen, *Ind. Eng. Chem. Res.*, 2018, **57**, 1790–1802.
23 E. A. Weiss, *Acc. Chem. Res.*, 2013, **46**, 2607–2615.
24 S. V. Kilina, P. K. Tamukong and D. S. Kilin, *Acc. Chem. Res.*, 2016, **49**, 2127–2135.

25 S. Kilina, D. Kilin and S. Tretiak, *Chem. Rev.*, 2015, **115**, 5929–5978.
26 Y. Hong, Y. Wu, S. Wu, X. Wang and J. Zhang, *Isr. J. Chem.*, 2019, **59**, 661–672.
27 C. M. Perez, D. Ghosh, O. Prezhdo, S. Tretiak and A. J. Neukirch, *J. Phys. Chem. Lett.*, 2021, **12**, 1005–1011.
28 B. Smith, M. Shakiba and A. V. Akimov, *J. Chem. Theory Comput.*, 2021, **17**, 678–693.
29 S. Kilina, S. Ivanov and S. Tretiak, *J. Am. Chem. Soc.*, 2009, **131**, 7717–7726.
30 K. A. Nguyen, P. N. Day and R. Pachter, *J. Phys. Chem. C*, 2010, **114**, 16197–16209.
31 S. A. Fischer, A. M. Crotty, S. V. Kilina, S. A. Ivanov and S. Tretiak, *Nanoscale*, 2012, **4**, 904–914.
32 M. D. Ben, R. W. A. Havenith, R. Broer and M. Stener, *J. Phys. Chem. C*, 2011, **115**, 16782–16796.
33 M. Imran, M. J. Saif, A. E. Kuznetsov, N. Idrees, J. Iqbal and A. A. Tahir, *RSC Adv.*, 2019, **9**, 5091–5099.
34 I. Dmitruk, R. V. Belosludov, A. Dmytruk, Y. Noda, Y. Barnakov, Y.-S. Park and A. Kasuya, *J. Phys. Chem. A*, 2020, **124**, 3398–3406.
35 L. Lystrom, A. Roberts, N. Dandu and S. Kilina, *Chem. Mater.*, 2021, **33**, 892–901.
36 T. Goldzak, A. R. McIsaac and T. Van Voorhis, *Nat. Commun.*, 2021, **12**, 890.
37 M. B. Teunis, M. Nagaraju, P. Dutta, J. Pu, B. B. Muhoberac, R. Sardar and M. Agarwal, *Nanoscale*, 2017, **9**, 14127–14138.
38 M.-Y. Huang, X.-B. Li, Y.-J. Gao, J. Li, H.-L. Wu, L.-P. Zhang, C.-H. Tung and L.-Z. Wu, *J. Mater. Chem. A*, 2018, **6**, 6015–6021.
39 W. Xia, J. Wu, J.-C. Hu, S. Sun, M.-D. Li, H. Liu, M. Lan and F. Wang, *ChemSusChem*, 2019, **12**, 4617–4622.
40 A. N. Beecher, R. A. Dziatko, M. L. Steigerwald, J. S. Owen and A. C. Crowther, *J. Am. Chem. Soc.*, 2016, **138**, 16754–16763.
41 O. Voznyy, *J. Phys. Chem. C*, 2011, **115**, 15927–15932.
42 O. Voznyy, S. M. Thon, A. H. Ip and E. H. Sargent, *J. Phys. Chem. Lett.*, 2013, **4**, 987–992.
43 A. J. Houtepen, Z. Hens, J. S. Owen and I. Infante, *Chem. Mater.*, 2017, **29**, 752–761.
44 I. du Fossé, S. C. Boehme, I. Infante and A. J. Houtepen, *Chem. Mater.*, 2021, **33**, 3349–3358.
45 M. L. del Puerto, M. L. Tiago and J. R. Chelikowsky, *Phys. Rev. Lett.*, 2006, **97**, 096401.
46 H. H.-Y. Wei, C. M. Evans, B. D. Swartz, A. J. Neukirch, J. Young, O. V. Prezhdo and T. D. Krauss, *Nano Lett.*, 2012, **12**, 4465–4471.
47 V. V. Albert, S. A. Ivanov, S. Tretiak and S. V. Kilina, *J. Phys. Chem. C*, 2011, **115**, 15793–15800.
48 A. Sheely, B. Gifford, S. Tretiak and A. Bishop, *J. Phys. Chem. C*, 2021, **125**, 9244–9252.
49 J. M. Azpiroz, J. M. Matxain, I. Infante, X. Lopez and J. M. Ugalde, *Phys. Chem. Chem. Phys.*, 2013, **15**, 10996–11005.
50 N. C. Anderson, M. P. Hendricks, J. J. Choi and J. S. Owen, *J. Am. Chem. Soc.*, 2013, **135**, 18536–18548.
51 E. Drijvers, J. De Roo, J. C. Martins, I. Infante and Z. Hens, *Chem. Mater.*, 2018, **30**, 1178–1186.
52 V. Barone and M. Cossi, *J. Phys. Chem. A*, 1998, **102**, 1995–2001.
53 M. Cossi, N. Rega, G. Scalmani and V. Barone, *J. Comput. Chem.*, 2003, **24**, 669–681.
54 V. N. Soloviev, A. Eichhöfer, D. Fenske and U. Banin, *J. Am. Chem. Soc.*, 2000, **122**, 2673–2674.
55 V. N. Soloviev, A. Eichhöfer, D. Fenske and U. Banin, *J. Am. Chem. Soc.*, 2001, **123**, 2354–2364.
56 A. Kasuya, R. Sivamohan, Y. A. Barnakov, I. M. Dmitruk, T. Nirasawa, V. R. Romanyuk, V. Kumar, S. V. Mamykin, K. Tohji, B. Jeyadevan, K. Shinoda, T. Kudo, O. Terasaki, Z. Liu, R. V. Belosludov, V. Sundararajan and Y. Kawazoe, *Nat. Mater.*, 2004, **3**, 99–102.
57 B. Tirloni, E. S. Lang and G. M. de Oliveira, *Polyhedron*, 2013, **62**, 126–132.
58 J. Jasieniak and P. Mulvaney, *J. Am. Chem. Soc.*, 2007, **129**, 2841–2848.
59 A. M. Smith and S. Nie, *Acc. Chem. Res.*, 2010, **43**, 190–200.
60 R. L. Martin, *J. Chem. Phys.*, 2003, **118**, 4775–4777.
61 F. L. Hirshfeld, *Theor. Chim. Acta*, 1977, **44**, 129–138.
62 C. B. Murray, D. J. Norris and M. G. Bawendi, *J. Am. Chem. Soc.*, 1993, **115**, 8706–8715.
63 M. J. Frisch, G. W. Trucks, H. B. Schlegel, G. E. Scuseria, M. A. Robb, J. R. Cheeseman, G. Scalmani, V. Barone, G. A. Petersson, H. Nakatsuji and X. Li, *Gaussian 16*, Gaussian Inc., Wallingford CT, 2016.
64 A. D. Becke, *J. Chem. Phys.*, 1993, **98**, 5648–5652.
65 C. Lee, W. Yang and R. G. Parr, *Phys. Rev. B: Condens. Matter Mater. Phys.*, 1988, **37**, 785–789.
66 R. Ditchfield, W. J. Hehre and J. A. Pople, *J. Chem. Phys.*, 1971, **54**, 724–728.
67 P. J. Hay and W. R. Wadt, *J. Chem. Phys.*, 1985, **82**, 270–283.
68 W. R. Wadt and P. J. Hay, *J. Chem. Phys.*, 1985, **82**, 284–298.
69 P. K. Tamukong, W. D. N. Peiris and S. Kilina, *Phys. Chem. Chem. Phys.*, 2016, **18**, 20499–20510.
70 Y. Cui, Z. Lou, X. Wang, S. Yu and M. Yang, *Phys. Chem. Chem. Phys.*, 2015, **17**, 9222–9230.
71 T. Lu and F. Chen, *J. Comput. Chem.*, 2012, **33**, 580–592.
72 N. M. O'boyle, A. L. Tenderholt and K. M. Langner, *J. Comput. Chem.*, 2008, **29**, 839–845.
73 K. Momma and F. Izumi, *J. Appl. Crystallogr.*, 2011, **44**, 1272–1276.

